Available online at www.sciencedirect.com

ScienceDirect

Proceedings of the Combustion Institute 37 (2019) 1521–1528

Proceedings of the Combustion Institute

www.elsevier.com/locate/proci

Flame propagation speed and Markstein length of spherically expanding flames: Assessment of extrapolation and measurement techniques

J. Beeckmann [a,*], R. Hesse [a], J. Schaback [a], H. Pitsch [a], E. Varea [b], N. Chaumeix [c]

[a] *Institute for Combustion Technology, RWTH Aachen University, Templergraben 64 Aachen D-52056 Germany*

[b] *CORIA-UMR 6614, Normandie Université, CNRS, INSA et Université de Rouen Av de l'Université, Saint Etienne du Rouvray 76800 France*

[c] *Institut de Combustion, Aérothermique, Réactivité et Environnement (ICARE), CNRS-INSIS, 1C Avenue de la Recherche Scientifique, Orléans Cedex 02 F-45071 France*

Received 1 December 2017; accepted 24 August 2018
Available online 2 November 2018

Abstract

Laminar burning velocities are of great importance in many combustion models as well as for validation and improvement of chemical kinetic schemes. Determining laminar burning velocities with high accuracy is quite challenging and different approaches exist. Hence, a comparison of existing methods measuring and evaluating laminar burning velocities is of interest. Here, two optical diagnostics, high speed tomography and Schlieren cinematography, are simultaneously set up to investigate methods for evaluating laminar flame speed in a spherical flame configuration. The hypothesis to obtain the same flame propagation radii over time with the two different techniques is addressed. Another important aspect is the estimation of flame properties, such as the unstretched flame propagation speed and Markstein length in the burnt gas phase and if these are estimated satisfactorily by common experimental approaches. Thorough evaluation of the data with several extrapolation techniques is undertaken. A systematic extrapolation approach is presented to give more confidence into results generated experimentally. The significance of the linear extrapolation routine is highlighted in this context. Measurements of spherically expanding flames are carried out in two high-pressure, high-temperature, constant-volume vessels at RWTH in Aachen, Germany and at ICARE in Orleans, France. For the discussion of the systematic extrapolation approach, flame speed measurements of methane / air mixtures with mixture Lewis numbers moderately away from unity are used. Conditions were varied from lean to rich mixtures, at temperatures of 298–373 K, and pressures of 1 atm and 5 bar.

Keywords: laminar burning velocity; flame propagation speed, spherical flames; tomography; Schlieren cinematography; extrapolation techniques

* Corresponding author.
E-mail address: jbeeckmann@itv.rwth-aachen.de (J. Beeckmann).

https://doi.org/10.1016/j.proci.2018.08.047
1540-7489

1. Introduction

Laminar burning velocities LBV are of great importance for turbulent combustion as well as validation and improvement of chemical kinetic schemes [1]. The experimental methodologies for fundamental flame speed determination involve flames that are either stationary, including conical, flat, and counter-flow flames or they are propagating with respect to a quiescent unburned mixture like spherically expanding flames [2].

Out of these methodologies, the spherically expanding flame configuration SEF either as a dual chamber concept with fixed pressure or the single chamber concepts has the advantage that it offers flexibility in terms of initial pressure, temperature, and gas composition [3]. Even though SEF studies started almost one hundred years ago [4], comparison between different experimental data sets is still challenging. Flame recording techniques (pressure trace, Schlieren cinematography, high speed shadowgraphy or tomography techniques) as well as chamber geometries may differ significantly from one setup to another [5]. Unfortunately, the intrinsic uncertainties associated with each setup are not well known. Hence, a comparison of existing methods for determining LBV based on different optical diagnostics and on different chamber geometries is required. For optical diagnostics, high-speed tomography or Schlieren imaging are the most developed techniques and find broad application. High-speed tomography allows determining the flame position based on the evaporation contour of oil droplets. Additionally, it provides direct measurements of local instantaneous LBV by extraction of the fresh gas velocity just ahead of the flame through particle image velocimetry (PIV) [6,7]. The Schlieren imaging technique on the other hand captures the flame location at the maximum gradient of the refractive index [8]. In theory, both imaging techniques should yield the same information regarding the expanding flame radius r_f over time t [9]. One question to be addressed: Do Schlieren and tomography experiments confirm that?

In common, the stretched propagation speed with respect to the burnt mixture s_b can be determined by the derivative $\mathrm{d}r_f/\mathrm{d}t$. The flame stretch rate κ is defined as the temporal change of a flame surface area A [10]. In case of an outwardly expanding spherical flame front, κ can be expressed as

$$\kappa = \frac{1}{A}\frac{\mathrm{d}A}{\mathrm{d}t} = \frac{2}{r_f}\frac{\mathrm{d}r_f}{\mathrm{d}t}. \tag{1}$$

The response of flames to weak stretch has been analysed on the basis of asymptotic theory. The burnt gas Markstein length $\mathcal{L}_b$ can be described as

$$s_b^0 - s_b = \mathcal{L}_b\kappa, \tag{2}$$

where s_b^0 is the unstretched flame speed with respect to the burnt mixture (hereafter referred to as the linear method, LM) [11].

Apart from LM, additional extrapolation techniques have been proposed to capture the non-linear behaviour for various reasons. The first reason is the non-linear behaviour of small flames at high stretch rate. Secondly, non-linear effects occur at low stretch for large flames with Lewis numbers significantly away from unity. These effects were discussed for varying fuels, e.g., hydrogen, methane, and n-heptane, especially for very lean/rich mixtures at ambient conditions.

Besides LM, in the present study, a common non-linear model is utilised to extract s_b^0 and $\mathcal{L}_b$, hereafter referred to as the non-linear method, NM. This technique has been discussed by Halter et al. [12] and is given as

$$\left(\frac{s_b}{s_b^0}\right)^2 \ln\left(\frac{s_b}{s_b^0}\right)^2 = -\frac{2\mathcal{L}_b\kappa}{s_b^0}. \tag{3}$$

It is based on an earlier work of Ronney and Sivashinsky [13]. A least-squares fit is applied to obtain the unknown parameters, s_b^0 and $\mathcal{L}_b$ for LM and NM. For completeness, Kelly and Law [14] proposed a slightly more accurate method for NM using an analytical solution based only on the temporal evolution of the flame radius. Chen [15] showed by data analysis from 1D spherically expanding flame simulations that depending on the mixture Lewis numbers, either NM for small or a non-linear model proposed by Frankel and Sivanshinsky [16] for large Lewis numbers is favoured. The latter model, under the assumption of large flame radii, shows a linear change with flame curvature.[1] Kelly et al. [17] relaxed the quasi-steady assumption of Eq. (3). They incorporated an unsteady term already noted by Ronney and Sivashinsky [13] in form of an expansion.[2] Recognising that differences among the aforementioned models start from the second-order inverse power of r_f, Wu et al. [18] proposed an extrapolation equation with a free parameter on the second-order term, which relies on experimental data to describe the curvature.[3] Liang et al. [19] identified the important role of finite flame thickness on highly stretched flames. They adopted the finite flame thickness δ^0 expression into the extrapolation. This is similar to Eq. (3), except for an additional term corresponding to the finite flame thickness.[4]

Looking at processing of experimental data, it is evident, that most data published for s_b^0 and $\mathcal{L}_b$

[1] Frankel and Sivashinsky: $\frac{s_b}{s_b^0} = 1 - \mathcal{L}_b\frac{2}{r_f}$.

[2] Kelly et al.: $\frac{s_b}{s_b^0}\left[1 + \frac{2\mathcal{L}_b}{r_f} + \frac{4\mathcal{L}_b^2}{r_f^2} + \frac{16\mathcal{L}_b^3}{3r_f^3} + o^4\left(\frac{\mathcal{L}_b}{r_f}\right)\right] = 1.$

[3] Wu et al.: $\frac{s_b}{s_b^0} = 1 - \frac{2\mathcal{L}_b}{r_f} + \frac{C}{r_f^2}$.

[4] Liang et al.: $\left(\frac{s_b}{s_b^0} + \frac{2\delta^0}{r_f}\right)\ln\left(\frac{s_b}{s_b^0} + \frac{2\delta^0}{r_f}\right) = -\frac{2(\mathcal{L}_b - \delta^0)}{r_f}$.

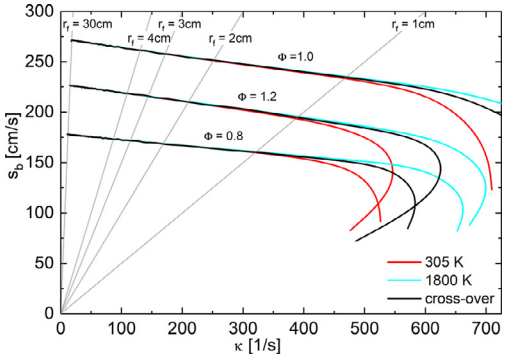

Fig. 1. Calculated propagation speed over stretch for methane / air flames based on different temperature iso-surfaces at $\phi = 0.8$, 1.0, and 1.2 at 1 atm and 298 K; flame iso-radii r_f at 1, 2, 3, 4, and 30 cm.

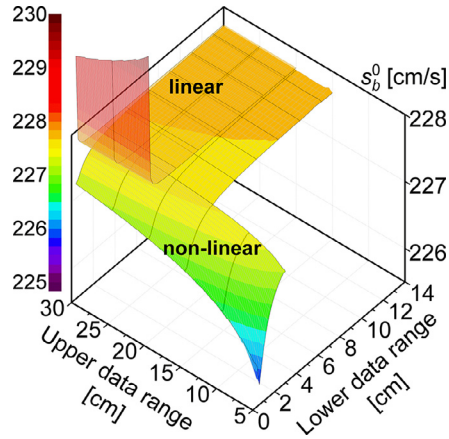

Fig. 2. Influence of data range variation on propagation speed of simulated spherically expanding methane / air flames evaluated with NM and LM at $\phi = 1.2$ at 298 K and 1 atm.

over the last years are obtained by NM, but results obtained by LM are sparse. In general, data used in this context are usually in the range from 1 to 3 cm, which is the data range of quasi-steady propagation. Even this data range is usually limited, e.g., due to ignition and/or facility effects, and alters the amount of data points available for extrapolation. The following questions need to be addressed: Is NM the right choice, is LM to be favoured, or perhaps a combination of both?

In this study, only flames with Lewis numbers moderately away from unity are considered. To emphasise a potential preference of LM, the authors computed the propagation speed over stretch for typical spherically expanding methane / air flames at standard conditions and different equivalence ratios up to flame radii of around 30 cm (details in Section 3). Computed flames are shown in Fig. 1. In addition to the temperature iso-surfaces, grey lines represent varying iso-radii r_f at 1, 2, 3, 4, and 30 cm. A transition is observed from an ignition phase of highly curved iso-surfaces at high stretch rates to the region where the flame propagation speed exhibits a linear dependence on stretch. In this region, the value of the propagation speed is insensitive to the reference position within the flame and the resulting Markstein lengths for all temperature iso-surfaces correspond to the burnt value in Eq. (2) [9].

This is elucidated in Fig. 2. Here, the result in unstretched flame propagation speed s_b^0 is given as a function of a varying data range used for extrapolation. The data range is defined by an upper and lower data range limit ranging from 5 to 30 cm and 1 to 5 cm, respectively. Results for both LM and NM are shown. Ultimately, the processing of the data range, according to the theory of weakly stretched flames, should yield the same results for LM and NM. This is achieved when a large initial flame radius is selected (40 mm) and the largest possible flame radius is used for the upper data range (300 mm). The results for LM and NM are identical with a minor deviation of 0.1 cm/s in the burnt. Unstretched flame propagation speeds s_b^0 are 227.77 cm/s and 227.68 cm/s. The Markstein lengths are also nearly identical with 0.861 mm and 0.813 mm

As already mentioned in the beginning, reliable data for s_b^0 and $\mathcal{L}$ are mandatory for kinetics modelling and for turbulent combustion models, for instance flamelet-type models [1]. The importance of stretch, which is represented by the Markstein length, has been pointed out by several authors, e.g., van Oijen et al. [20] and Trisjono et al. [21]. The temperature iso-surface at the maximum heat release or the inner layer temperature serves as a reference for tracking the flame propagation. However, due to strong curvature and strain effects in turbulent flames, Markstein lengths attributed to the individual propagation speed are not independent of the respective temperature iso-surface as depicted in Fig. 1. Hence, a Markstein length attributed to the correct reference temperature must be used, which is in most models the cross-over temperature [1].

The previously addressed questions lead to the main objectives of this work, which are i/ to compare if same results are obtained from the two optical diagnostic methods in r_f; ii/ to identify regions of extrapolations where the data range is sufficient and if the linear and/or the non-linear model for extrapolation is suitable; and iii/ to provide a workflow for robust estimation of propagation speed and Markstein length data in the burnt for mixtures with a Lewis numbers moderately away from unity.

The limitation of data range is responsible for major uncertainty in cases of Lewis numbers away from unity since the sensitivity to linear and non-linear parameters are increased. Therefore, the

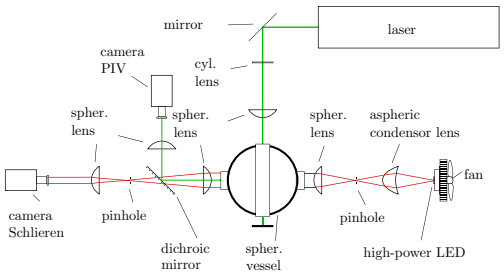

Fig. 3. Schematic of Schlieren/tomography arrangement.

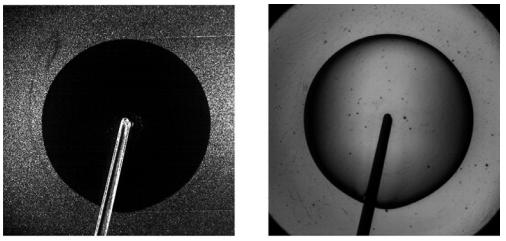

$s_b = 179.6\,\mathrm{cm/s}$ $\kappa = 286\,1/\mathrm{s}$

$s_b = 174.0\,\mathrm{cm/s}$ $\kappa = 291\,1/\mathrm{s}$

Fig. 4. Spherical tomography (left) and Schlieren (right) methane / air flame images; $\phi = 1.1$, at 2.5 bar, and 298 K; $t = 7.4$ ms after ignition.

paper corroborates the previous study of Wu er al. [18], where hydrogen and heptane flames were studied.

The work is structured as follows. The next section presents the experimental framework together with the optical diagnostics for the experimental facilities at RWTH in Aachen, Germany, and ICARE in Orleans, France. Section 3 gives the simulation framework. Subsequently, the results are presented and discussed in Section 4. Section 5 summarises the content of this work and discusses the meaning of flame propagation speed and the Markstein length data with respect to the optical diagnostics and the extrapolation schemes.

2. Experimental framework

Experiments at RWTH were performed using the closed-vessel method combined with two different optical diagnostics. The first one consists of a Schlieren cinematography setup. It is comparable to the one described by Beeckmann et al. [22]. The second RWTH arrangement provides a simultaneous acquisition system. It utilises the standard Schlieren setup and a tomography setup, comparable to the one described by Varea et al. [6]. The simultaneous setup is shown schematically in Fig. 3. The internal shape of the combustion vessel is spherical with an inner diameter of 100 mm; quartz windows with an optical accessibe radius of 25 mm are positioned on opposite sides [22]. The stainless steel spherical vessel at ICARE in Orleans has an inner radius of 238 mm and optical access with a radius of 50 mm. For image acquisition, a high speed Schlieren arrangement is used. More details are found in Comandini et al. [23].

A summary table of the key features of RWTH and ICARE is given in the Supplemental material. In addition, a Figure comparing the RWTH setup with reference data for verification is given together with more details on the RWTH setup with respect to Schlieren and tomography, and the temperature distribution.

In the simultaneous Schlieren/tomography setup at RWTH, methane / air flames with an equivalence ratio of 1.1 at 2.5 bar and 298 K were investigated. Additionally at RWTH, methane / air flames were measured in the standard setup over a wide range of equivalence ratios (0.7–1.3), and at 1 atm to 5 bar and 298 K and 373 K, to compare the influence of LM and NM on Markstein lengths and flame speeds. At ICARE, methane/air flames were measured at an equivalence ratio of 1.3 at ambient conditions. Experimental conditions were set up with dehumidified compressed air, which consists of 20.94 % oxygen, 78.13 % nitrogen, and 0.93 % argon. Methane is obtained from Westfalen gas, grade 5.5.

A set of two typical images of the spherical flame evolution recorded with both optical diagnostics is shown in Fig. 4. Images are taken at 7.4 ms after ignition. In addition, the flame propagation speed s_b and the stretch rate κ are given.

3. Simulation framework

In this work, numerical simulations were performed using the FlameMaster software package [24]. Stationary laminar flame speed calculations were calculated with the 1D premixed, freely propagating flame module. Spherically propagating flames were simulated using the 1D transient flame propagation module. For the calculation of spherically expanding flames, the set of conservation equations in one-dimensional geometries is described in Maas and Warnatz [25]. For the computation of planar and spherically expanding flames, the GRI 3.0 [26] detailed kinetic mechanism with 325 elementary chemical reactions and 53 species was used.

4. Results and discussion

In the first part of this section, potential differences between the optical measurement techniques are examined by simultaneously measuring the spherically expanding flames with high

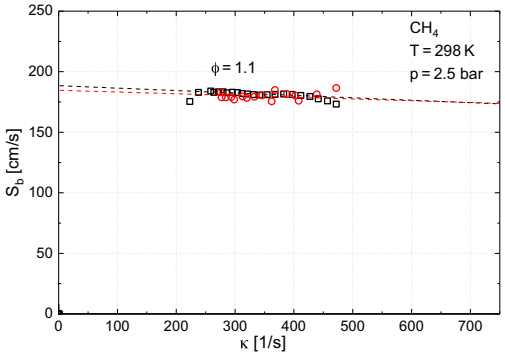

Fig. 5. Measured propagation speed over stretch for methane / air flames; PIV ○, Schlieren □, $\phi = 1.1$ at 2.5 bar and 298 K; LM.

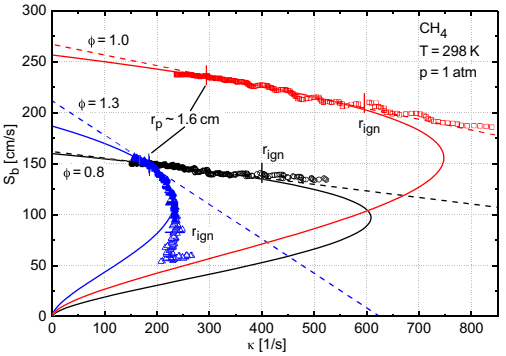

Fig. 6. Measured propagation speed over stretch for methane / air flames for $\phi = 0.8$ ○, 1.0 □, and 1.3 ▽, at 1 atm and 298 K; NM ——— and LM - - - -; pressure limit r_p and ignition limit r_{ign}.

speed tomography and Schlieren cinematography. In the second part, a combined extrapolation approach is suggested to assure robust results for unstretched flame propagation speed and Markstein length with respect to the burnt.

4.1. Optical measurement techniques

With the combined Schlieren/tomography setup as described in Section 2, s_b can be measured experimentally at an isotherm of evaporation for the PIV tracer of around 580 K and for Schlieren at a specific optical gradient index of around 480 K. Looking again at Fig. 4 for the present experimental condition, the flame radii of the Schlieren and the PIV have nearly the same temporal flame radius evolution. This is also illustrated in Fig. 5 for the propagation speed plotted against the stretch rate. The evolution of the data is almost linear. Both techniques yield nearly identical results for flame propagation speed and Markstein length of around 186 cm/s and 0.2 mm. Due to the small difference in the temperature iso-surface between Schlieren and tomography, varying effects of non-linear nature will be hard to visualise and can be only discriminated at very high stretch rates. The results confirm, that both optical techniques yield identical results within the experimental uncertainty. This leads to the next objective of this study to possibly identify a region of extrapolation where the data range is sufficient to ensure correct estimation of flame properties in the burnt.

4.2. Systematic extrapolation approach

In this subsection, a systematic approach is proposed to obtain robust results for the unstretched propagation speed and the Markstein length with respect to the burnt. The approach aims to be insensitive to the influence of temperature iso-surfaces. Usually after image processing, the standard workflow is to plot the flame propagation speed against the stretch rate. This is illustrated in Fig. 6 for lean, rich, and stoichiometric methane / air mixtures at ambient conditions. The temporal evolution of the flame goes from high to low stretch values. Symbols indicate the results of the post-processed flame images. A non-linear behaviour in flame speed evolution against stretch depending on the equivalence ratio is observed for high stretch rates, especially for $\phi = 1.3$. Limits for the extrapolation range in terms of minimum and maximum flame radius need to be identified. The aim is to evaluate any experimental data with a smooth spherical flame front. Often, small artefacts are visible on the flame surface resulting from the ignition process, but these do not significantly increase during the investigated flame radius evolution. Their influence on the resulting flame speed is negligible. The spark's influence itself as a result of the ignition process onto the flame speed evaluation is avoided by choosing flame radii larger than a specifically defined ignition radius r_{ign} for post-processing [27]. r_{ign} is marked for each measurement in Fig. 6 by a vertical marker. The extrapolation is applied for data where the chamber pressure remains nearly constant. Here, the pressure rise limit for post-processing is set to 1%, marked for each measurement in Fig. 6 by an additional vertical marker with the corresponding flame radius r_p. The extrapolation is performed from the biggest flame radius r_p towards small, higher curved flames limited by r_{ign}. An additional constraint to the extrapolation range is given if the influence of cellular structures on the flame surface area is appearing earlier than the pressure threshold. The development of cellular structures and number of cells is enhanced with increasing flame radii especially by mixture Lewis numbers significantly below unity and by increasing initial chamber pressure. Therefore, only flame radii are used for extrapolation, not showing wrinkling of the flame contour nor cell splitting and which are within the pressure

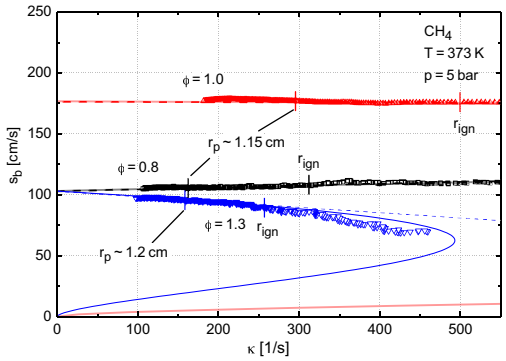

Fig. 7. Measured propagation speed over stretch for methane / air flames for $\phi = 0.8$ □, 1.0 △, and 1.3 ▽, at 1 atm and 298 K; NM ▬ and LM - - -; pressure limit r_p and ignition limit r_{ign}.

limit. In Fig. 6, the dashed line represent LM and solid lines NM. Results obtained for s_b^0 and $\mathcal{L}_b$ are summarised in Table A.2 of the Supplemental material.

LM and NM extrapolation yield for the lean mixture the same results. But with increasing equivalence ratio, the discrepancies between LM and NM increase until the linear extrapolation routine cannot be applied for fuel rich mixtures. No linear region of the flame evolution can be identified any more. It is even questionable if the available data range is large enough to provide reliable data with NM and the question is how to proceed. A way out of this dilemma is to only use data sets, for which results in LM and NM are the same.

One option to further minimise the discrepancy between the extrapolation techniques, is the increase in initial chamber pressure resulting in reduced flame propagation speeds. For an increased initial pressure of 5 bar at 373 K, as shown in Fig. 7, LM and NM yield nearly identical results for the entire range in equivalence ratio. Also in the case of negative Markstein lengths, $\phi = 0.8$, the extrapolation routines give identical results. Thus, the results for the burnt propagation speed and Markstein length are insensitive to variable temperature iso-surfaces. The results are summarised in Table A.2. The negative influence of cellular structures due to hydrodynamic instabilities caused by the decrease in flame thickness can be suppressed with dilution and replacement of nitrogen by argon [28]. Buoyancy may also affect the results and must be thoroughly checked. This can be achieved by tracking the centre position of the spherical flame over time.

In general, the applicability of the extrapolation methodologies can be further assessed by a data range variation of the upper and lower radius limits used for extrapolation. One example of the routine has already been shown in Fig. 2 for very large simulated methane / air flames. Apparently, this routine has been developed on the basis of results, suggestions, and private communication accomplished within an international collaboration starting already back in 2012 [29,30]. Here, the most challenging case at $\phi = 1.3$ has been chosen. Figure 8 illustrates the effect on the unstretched flame propagation speed depending on the radius domain used with NM for a methane / air flames. The lower radius domain is varied from 4 to 10 mm and the upper domain from 12 to 20 mm. Subfigure (a) shows the rich case at 1 atm and 298 K. Starting with the biggest radius in the upper limit range and going towards smaller radii, while keeping the lower radius above 7 mm, no region yields results of small variance. This indicates, that the result is not reliable for rich mixtures at ambient pressure.

The radius domain variation is applied now at the same equivalence ratio and temperature but at increased pressure of 5 bar. Subfigure (b) shows NM. The variance in unstretched flame speed over

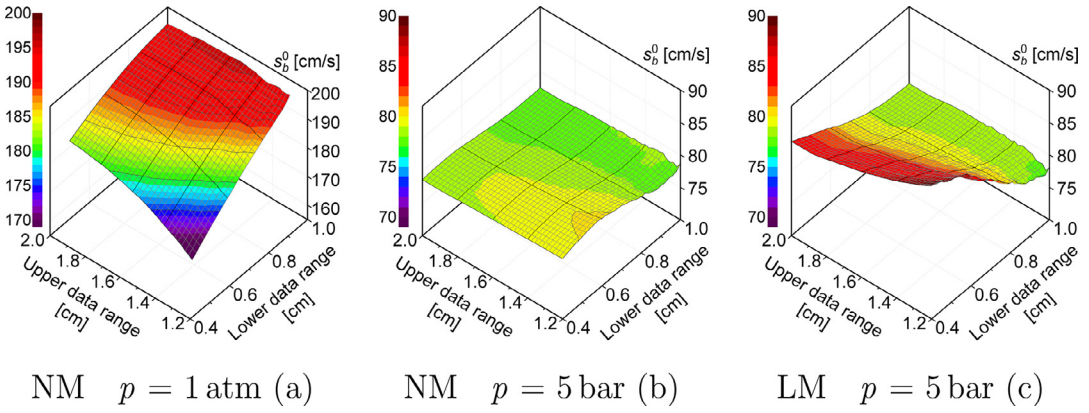

Fig. 8. Influence of data range variation on propagation speed of spherically expanding flames of rich ($\phi = 1.3$) methane / air flames at $T_i = 298K$; evaluated with NM and LM 1 atm and 5 bar; RWTH setup.

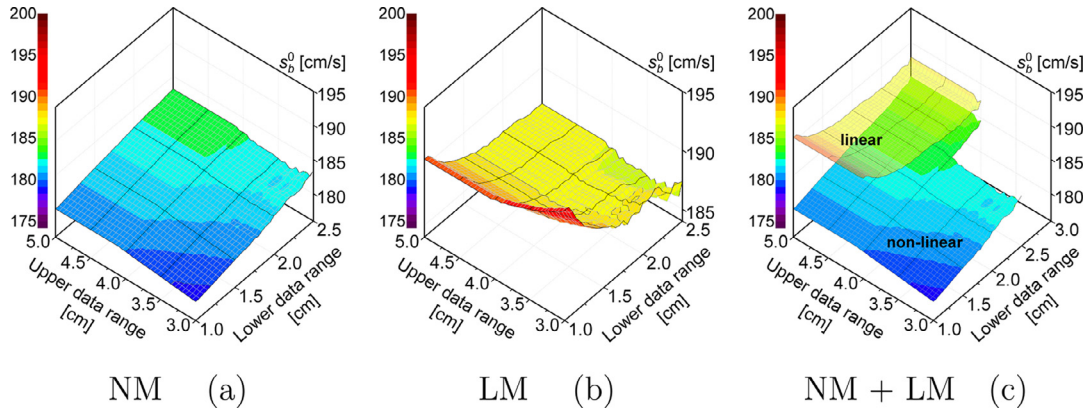

Fig. 9. Influence of data range variation on propagation speed of spherically expanding flames of rich ($\phi = 1.3$) methane / air flames at 298 K; evaluated with NM and LM at 1 atm; ICARE setup.

a wide applicable data range is found to be well below 2 cm/s. The lower data range is above 7 mm and the upper limit ranges between 20 and 14 mm with the non-linear extrapolation routine. The unstretched value s_b^0 is within this data range 78 cm/s and has a variance less than 2.5%. Is this result also independent of changing temperature isosurfaces? For affirmation, another data range variation applying the LM routine should also lead to a result with small variance in s_b^0. Ideally, it should be the same as the one from the non-linear routine. The linear variation for exactly the same 5 bar case is shown in subfigure (c). Here, the result of the unstretched value s_b^0 is 78 cm/s. This is identical to the result obtained by NM. Variance within the data range is 1 cm/s, which is less than 1.5 % of the unstretched value. This again shows that by adequately increasing the initial pressure, the variance in extrapolation can be significantly minimised yielding more robust results.

Coming back to the one atmosphere case at rich mixture, where the discrepancies are most prominent. The results by the RWTH vessel indicate that the spread between the two extrapolation techniques becomes bigger until it is recommended only to consider data under big uncertainties.

What will now happen if chamber size and the optically accessible flame radius is increased? Therefore, experimental data obtained by the chamber of ICARE in Orleans are used. Due to the large chamber radius of 238 mm, the flame propagation within the maximum accessible flame radius of 48.5 mm is measured without any observable pressure increase. Again, a data range variation for LM and NM is performed. It is shown in Fig. 9, subfigure (a) for NM and subfigure (b) for LM. This time, the variation in radius is chosen from 3 to 5 cm for the upper data range and from 1 to 3.5 cm for the lower data range. The unstretched flame speed s_b^0 is for LM and NM nearly identical with 186 cm/s and 183 cm/s, respectively (variance of less than 1 %). The corresponding Markstein length in the burnt gives 0.23 mm and 0.16 mm, respectively. Figures for the Markstein length data range variation are given in the Supplemental material. Clearly, it is seen now that both techniques tend for large data range toward same results. Both graphs are incorporated together in subfigure (c). Data ranges used elsewhere for experimental evaluation, e.g., 1–3 cm, would give in this case a deviation from 193 cm/s with LM to around 179 cm/s with NM. This is a spread of around 8 %. Thus, the discrepancies are not acceptable. This strongly indicates that experimental data should be assessed carefully, especially with respect to data range evaluation. It also proofs the consistency of the proposed workflow.

It is recommended for future flame speed and Markstein length evaluation, that results should be always provided for both LM and NM with respect to the burnt. In addition, s_b versus κ raw data and the extrapolation limits r_{ign} and r_p should be always provided.

5. Concluding remarks

Quite a few extrapolation techniques have appeared over the last years which describe non-linear behaviour of highly stretched flames in spherically expanding flame experiments. These extract unstretched flame propagation speed and Markstein length. Here, extrapolation limits with respect to ignition effects and isobaricity are revisited for mixture Lewis numbers moderately away from unity. The applicability of the extrapolation techniques is assessed for unstretched laminar flame speed and Markstein length with respect to the burnt. Simultaneous measurements of spherically expanding flames by Schlieren and tomography have been performed to guarantee that different techniques yield nearly identical results.

A framework is established to robustly evaluate experimental data. In general, experimental conditions must be chosen such that a large enough data range is available to perform linear and nonlinear extrapolation routines. Data range variations must yield results of small variance over a wide data range. Hence, final results for extrapolations should be nearly identical. If results do not match, the difference should be considered an uncertainty of the data evaluation.

Acknowledgements

This work was performed as part of the Cluster of Excellence "Tailor-Made Fuels from Biomass" funded by the German federal and state governments.

Supplementary material

Supplementary material associated with this article can be found, in the online version, at doi:10.1016/j.proci.2018.08.047.

References

[1] N. Peters, *Turbulent Combustion*, Cambridge University Press, 2000. Cambridge Books Online.
[2] F.N. Egolfopoulos, N. Hansen, Y. Ju, K. Kohse-Höinghaus, C.K. Law, F. Qi, *Prog. Energy Combust. Sci.* 43 (2014) 36–67.
[3] S.D. Tse, D.L. Zhu, C.K. Law, *Proc. Combust. Inst.* 28 (2) (2000) 1793–1800.
[4] E.F. Fiock, C.F. Marvin, *Chem. Rev.* 21 (3) (1937) 367–387.
[5] Z. Chen, *Combust. Flame* 162 (2015) 2442–2453.
[6] E. Varea, V. Modica, A. Vandel, B. Renou, *Combust. Flame* 159 (2) (2012) 577–590.
[7] S. Balusamy, A. Cessou, B. Lecordier, *Exp. Fuids* 50 (2011) 1109–1121.
[8] F.J. Weinberg, *Optics of Flames*, Butterworths, 1963.
[9] G.K. Giannakopoulos, A. Gatzoulis, C.E. Frouzakis, M. Matalon, *Combust. Flame* 162 (4) (2015) 1249–1264.
[10] F.A. Williams, *AGARD Conference Proceeding* 164 (1975).
[11] M. Matalon, B.J. Matkowsky, *J. Fluid Mech.* 124 (1982) 239–259.
[12] F. Halter, T. Tahtouh, C. Mounaïm-Rouselle, *Combust. Flame* 157 (10) (2010) 1825–1832.
[13] P.D. Ronney, G.I. Sivashinsky, J. Appl, *SIAM . Math* 49 (4) (1989) 1029–1046.
[14] A.P. Kelley, C.K. Law, *Combust. Flame* 156 (9) (2009) 1844–1851.
[15] Z. Chen, *Combust. Flame* 158 (2) (2011) 291–300.
[16] M.I. Frankel, G. Sivashinsky, *Combust. Sci. Technol.* 31 (1983) 131–138.
[17] A.P. Kelley, J.K. Bechtold, C.K. Law, J. Fluid, *Mech.* 691 (2012) 26–51.
[18] F. Wu, W. Liang, Z. Chen, Y. Ju, C.K. Law, *Proc. Combust. Inst.* 35 (1) (2015) 663–670.
[19] W. Liang, F. Wu, C.K. Law, *Proc. Combust. Inst.* 36 (1) (2017) 1137–1143.
[20] J.A.V. Oijen, L.P.H. De Goey, *Combust. Theor. Model.* 6 (3) (2002) 463–478.
[21] P. Trisjono, K. Kleinheinz, E.R. Hawkes, H. Pitsch, *Combust. Flame* 174 (2016) 194–207.
[22] J. Beeckmann, L. Cai, H. Pitsch, *Fuel* 117 (2014) 340–350. Part A.
[23] A. Comandini, T. Dubois, S. Abid, N. Chaumeix, *Energy Fuels* 28 (1) (2014) 714–724.
[24] H. Pitsch, *FlameMaster: A C++ computer program for 0D combustion and 1D laminar flame calculations* (1998).
[25] U. Maas, J. Warnatz, *Combust. Flame* 74 (1) (1988) 53–69.
[26] G. Smith, D. Golden, M. Frenklach, et al., GRI-Mech 3.0.University of California, CA, www.me.berkeley.edu/gri_mech/.
[27] Z. Chen, M.P. Burke, Y. Ju, *Proc. Combust. Inst.* 32 (1) (2009) 1253–1260.
[28] S. Yang, X. Yang, F. Wu, et al., *Proc. Combust. Inst.* 36 (1) (2017) 491–498.
[29] J. Beeckmann, N. Chaumeix, P. Dagaut, et al., *European Combustion Meeting* (2013).
[30] J. Goulier, D. Nativel, N. Chaumeix, N. Meynet, *European Combustion Meeting* (2013).